Miner Deposita (2011) 46:257–271
DOI 10.1007/s00126-010-0324-5

ARTICLE

Pingüino In-bearing polymetallic vein deposit, Deseado Massif, Patagonia, Argentina: characteristics of mineralization and ore-forming fluids

Sebastián M. Jovic · Diego M. Guido · Isidoro B. Schalamuk · Francisco J. Ríos · Colombo C. G. Tassinari · Clemente Recio

Received: 22 July 2009 / Accepted: 8 December 2010 / Published online: 8 January 2011

Abstract The Pingüino deposit, located in the low sulfidation epithermal metallogenetical province of the Deseado Massif, Patagonia, Argentina, represents a distinct deposit type in the region. It evolved through two different mineralization events: an early In-bearing polymetallic event that introduced In, Zn, Pb, Ag, Cd, Au, As, Cu, Sn, W and Bi represented by complex sulfide mineralogy, and a late Ag–Au quartz-rich vein type that crosscut and overprints the early polymetallic mineralization. The indium-bearing polymetallic mineralization developed in three stages: an early Cu–Au–In–As–Sn–W–Bi stage (Ps_1), a Zn–Pb–Ag–In–Cd–Sb stage (Ps_2) and a late Zn–In–Cd (Ps_3). Indium concentrations in the polymetallic veins show a wide range (3.4 to 1,184 ppm In). The highest indium values (up to 1,184 ppm) relate to the Ps_2 mineralization stage, and are associated with Fe-rich sphalerites, although significant In enrichment (up to 159 ppm) is also present in the Ps_1 paragenesis associated with Sn-minerals (ferrokesterite and cassiterite). The hydrothermal alteration associated with the polymetallic mineralization is characterized by advanced argillic alteration within the immediate vein zone, and sericitic alteration enveloping the vein zone. Fluid inclusion studies indicate homogenisation temperatures of 308.2–327°C for Ps_1 and 255–312.4°C for Ps_2, and low to moderate salinities (2 to 5 eq.wt.% NaCl and 4 to 9 eq.wt.% NaCl, respectively). $\delta^{34}S$ values of sulfide minerals (+0.76‰ to +3.61‰) indicate a possible magmatic source for the sulfur in the polymetallic mineralization while Pb isotope ratios for the sulfides and magmatic rocks ($^{206}Pb/^{204}Pb$, $^{207}Pb/^{204}Pb$ and $^{208}Pb/^{204}Pb$ ratios of 17.379 to 18.502; 15.588 to 15.730 and 38.234 to 38.756, respectively) are consistent with the possibility that the Pb reservoirs for both had the same crustal source. Spatial relationships, hydrothermal alteration styles, S and Pb isotopic data suggest a probable genetic relation between the polymetallic mineralization and dioritic intrusions that could have been the source of metals and hydrothermal fluids. Mineralization paragenesis, alteration mineralogy, geochemical signatures, fluid inclusion data and isotopic data, confirm that the In-bearing polymetallic mineralization from Pingüino deposit is a distinct type, in comparison with the well-known epithermal low sulfidation mineralization from the Deseado Massif.

Editorial handling: Noel White, Thomas Bissig and Rolf Romer

S. M. Jovic · D. M. Guido · I. B. Schalamuk
Instituto de Recursos Minerales, Facultad de Ciencias Naturales y Museo, Universidad Nacional de La Plata,
Paseo del Bosque s/n,
B1900FWA La Plata, Argentina

S. M. Jovic (✉) · D. M. Guido · I. B. Schalamuk
Consejo Nacional de Investigaciones Científicas y Técnicas,
La Plata, Argentina
e-mail: sjovic@inremi.unlp.edu.ar

F. J. Ríos
Laboratório de Inclusões Fluidas e Metalogênese,
Centro de Desenvolvimento da Tecnologia Nuclear,
Avenida Pres. Antônio Carlos 6627, Campus da UFMG,
Belo Horizonte 31270-901, Brazil

C. C. G. Tassinari
Centro de Pesquisas Geocronológicas, Instituto de Geociências,
Universidade de São Paulo,
Rua do Lago 562, Cidade Universitária,
São Paulo 05508-080, Brazil

C. Recio
Servicio General de Análisis de Isótopos Estables,
Facultad de Ciencias, Universidad de Salamanca,
Plaza de los Caídos s/n,
37008 Salamanca, Spain

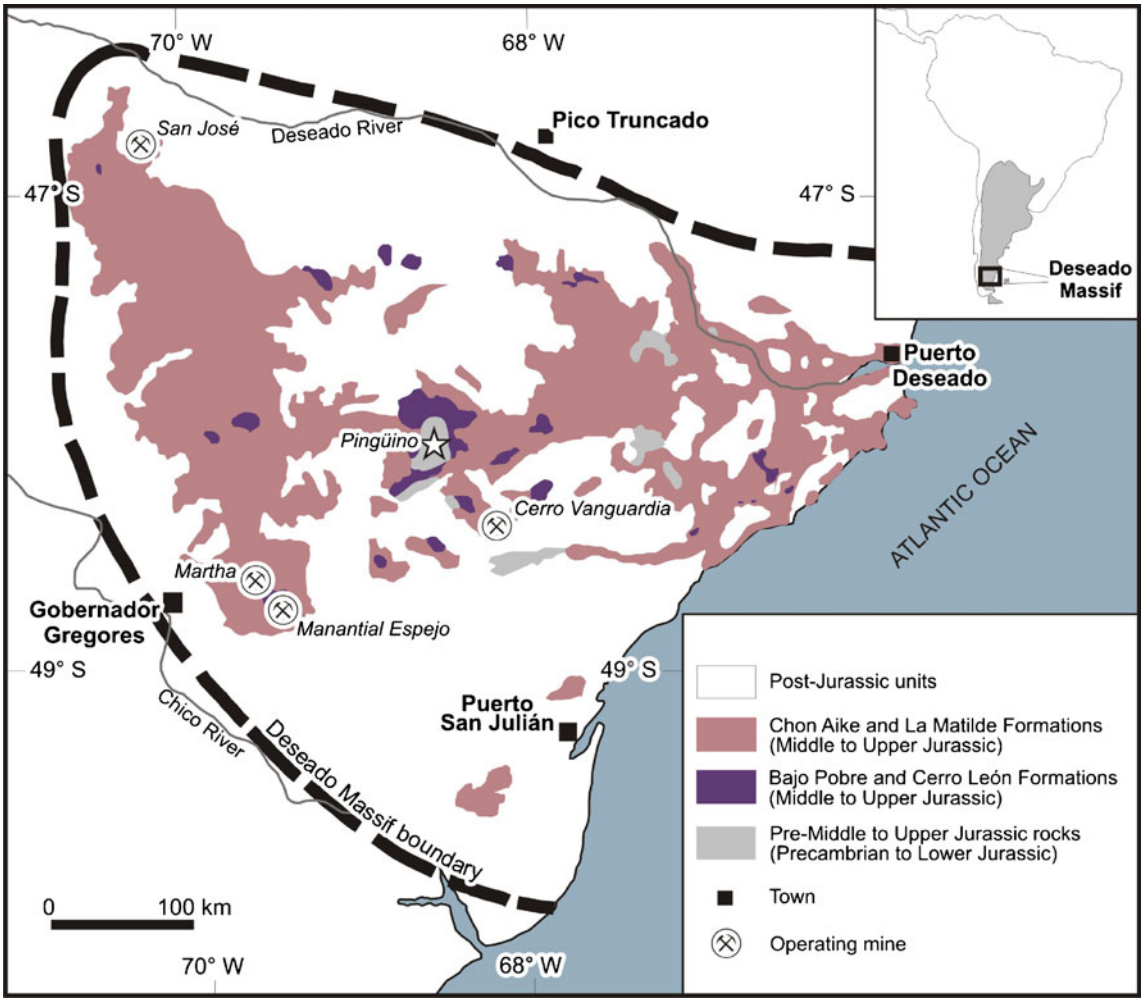

Fig. 1 Simplified geological map of the Deseado Massif and location of the mines and Pingüino deposit (Modified from Páez et al. 2010)

Keywords Polymetallic mineralization · Fluid characterization · Indium · Deseado Massif · Argentina

Introduction

The Pingüino In-bearing polymetallic vein deposit is the first indium occurrence found in Patagonia, Argentina, where Au–Ag deposits are more widely known. Located in the central portion of the low sulfidation epithermal metallogenetical province of the Deseado Massif (Fig. 1), Pingüino represents an atypical deposit in the region (Guido et al. 2005), characterized by the presence of two different vein types, namely early polymetallic sulfide-rich veins and late quartz-rich veins. The sulfide-rich veins contain In Zn, Pb, Ag, Au, Cu, Sn, W and Bi, hosted by complex sulfide mineralogy (Jovic et al. 2005; Crespi et al. 2006). The quartz-rich veins have high Ag, Au values and Ag/Au ratios and crosscut the early polymetallic sulfide-rich veins, suggesting the coincidence of the two different mineralization styles in the same fault system. The quartz-rich veins have similar characteristics to the typical low sulfidation type mineralization from the Deseado Massif (Jovic et al. 2008b, 2009, 2010).

Indium deposits are rare, little is known about potential alternative sources of this element which is used in the production of solar cells. High indium contents have been reported from metamorphosed sediment-hosted deposits (Burke and Kieft 1980), low-temperature Pb–Zn vein deposits (Palero-Fernández and Martín-Izard 2005), skarns (Ishihara et al. 2006), VHMS deposits and the present-day exhalative equivalents (Binns and Scott 1993; Fouquet et al. 1993; Huston et al. 1995; Schwarz-Schampera and Herzig 1997; Serranti et al. 2002; Benzaazoua et al. 2003; Ishihara et al. 2006), epithermal veins (Carrillo-Rosúa et al. 2008) and polymetallic veins associated with intrusions (Seifert 1999; Tsushima et al. 1999; Lenharo et al. 2002;

Ishihara et al. 2006; Zhang et al. 2006; Lerouge et al. 2007). Among them, the most economically interesting deposits are probably some Sn-bearing Pb–Zn deposits (Qian et al. 1998; Zhang et al. 2007). Indium can be concentrated either as indium minerals (roquesite ($CuInS_2$), laforetite ($AgInS_2$), indite ($FeIn_2S_4$), petrukite ($(Cu,Fe,Zn)_3(Sn,In)S_4$) and sakuraite ($(Cu,Fe,Zn,Ag)_3(Sn,In)S_4$)), though these are extremely rare worldwide, or as a trace element in the structure of other minerals particularly sphalerite, chalcopyrite (Boorman and Abbott 1967; Kieft and Damman 1990), digenite (Boorman and Abbott 1967), stannite (Cu_2FeSnS_4) (Boorman and Abbott 1967), ferrokesterite-kesterite ($Cu_2(Fe,Zn)SnS_4$) and cassiterite (Plimer et al. 1991; Shwarz-Schampera and Herzig 2002; Gorelikova et al. 2006).

Indium-rich polymetallic vein deposits are generally structurally controlled and occur within faults, fault systems, and vein breccia zones developed in clastic sedimentary rocks or magmatic dominated terranes. They include lead–zinc–silver, copper–zinc–lead–silver–tin, and tin–tungsten-base metal-dominated deposits. Polymetallic vein deposits may contain considerable and often economic Indium concentrations and are among the most important Indium producers worldwide (Shwarz-Schampera and Herzig 2002). Ohta (1995) studied the genesis of Indium-polymetallic deposits comparing different deposits from Japan (Toyoha, Ikuno-Akenobe, etc.) and Bolivia (Bolivar, Huari-Huari etc.). This style of mineralization is characterized by sulfide veins with Au, As, Cu, Sn, In, W, Bi Zn, In, Pb, Cd, Ag, Cu, a complex sulfide mineralogy, an important structural control, presence of intermediate to acid shallow intrusions associated with organic matter-rich sediments, and formation temperatures between 200° and 400°C. Seifert and Sandmann (2006) studied In-rich polymetallic veins from the Freiberg district, Germany, defining temperatures between 250° and 410°C and a genetic relationship between mineralized veins and the intrusion of lamprophyric dykes, also indicating a magmatic source for the hydrothermal fluids. Shwarz-Schampera and Herzig (2002) defined formation temperatures between 250° and 380°C for In-rich polyme-

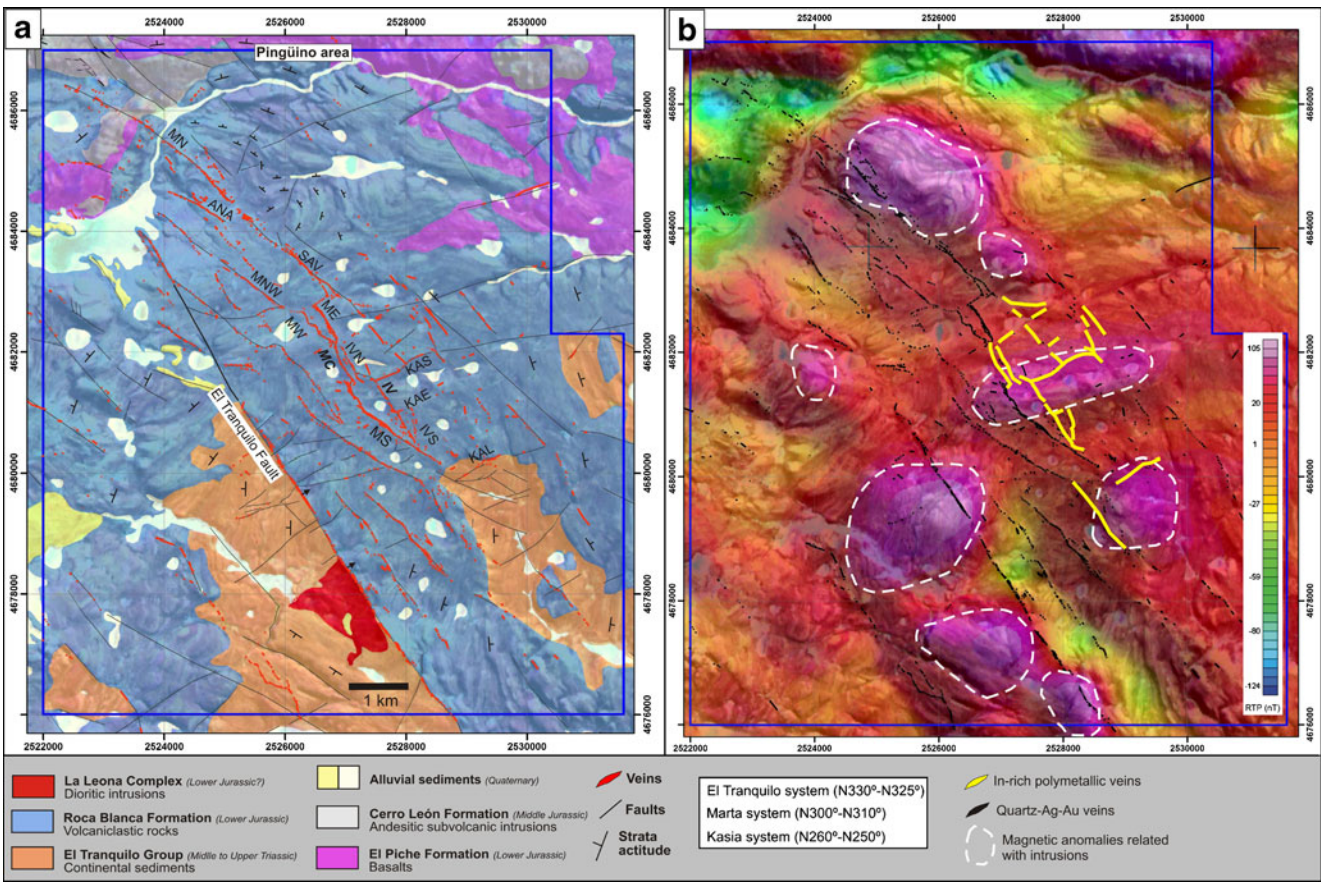

Fig. 2 **a** Simplified geological map of Pingüino deposit superimposed on a Landsat TM image. *MN* Marta Norte, *ANA* Ana, *SAV* Savary, *MNW* Marta Noroeste, *ME* Marta Este, *MW* Marta Oeste, *MC* Marta Centro, *IVN* Ivonne Norte, *IV* Ivonne, *KAS* Kasia, *MS* Marta Sur, *IVS* Ivonne Sur, *KAL* Kalia. **b** Regional magnetometric map superimposed on a Landsat TM image, showing important total magnetic field reduced to pole (RTP in nT) anomalies (*red–violet*) that responds to not outcropping subvolcanic bodies from La Leona Complex and the spatial relation between the sulfide veins and the subvolcanic bodies (Modified from Peñalva et al. 2008)

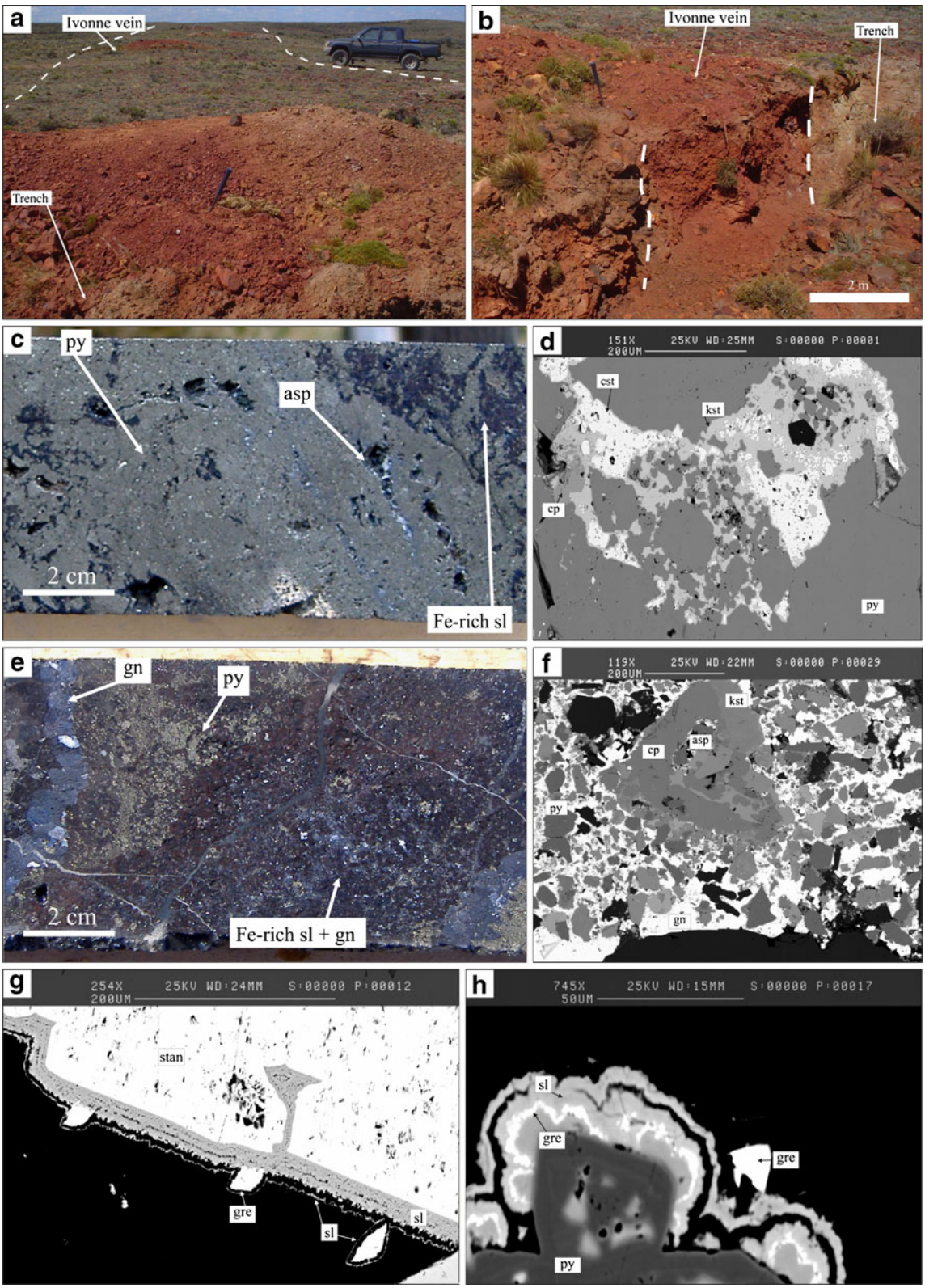

tallic vein deposits and genetic relations with intermediate to felsic subvolcanic intrusions.

Ohta (1995) based their mineralization model on the local reduction of organic matter within sedimentary rocks close to the upper parts of I-type magnetite series intrusions, resulting in the concentration of In and other elements such as Sn, Bi, W, Sb, As and Ga in the hydrothermal fluids. Mixing of those fluids with meteoric

◀**Fig. 3** **a** and **b** Fe-rich gossan from the Ivonne vein. **c** Drill hole core HQ diameter sample (65 mm, drill hole 102, −53.3 m depth) from the Ivonne vein showing Ps_1 pyrite and arsenopyrite crosscut by Ps_2 Fe-rich sphalerite and galena. **d** Backscattered electron image from Ivonne vein showing Ps_1 pyrite (*py*) and chalcopyrite (*cp*) crystals brecciated by cassiterite (*cst*) and ferrokësterite (*kst*). **e** Drill hole core HQ diameter sample of banded Fe-rich sphalerite and galena breccia (Ps_2) with pyrite clasts (Ps_1) from Marta Centro vein (drill hole 53, −54.2 m depth). **f** Backscattered electron image of a sample from the Marta Centro vein showing Ps_2 galena (*gn*) breccia with py, cp and kst clasts. **g** Backscattered electron image of a sample from the Ivonne vein where Ps_3 stannite (*stan*) and idiomorphic greenockite (*gre*) crystals are surrounded by botryoidal banded Fe-poor sphalerite (*sl*). **h** Backscattered electron image of a sample from the Ivonne vein, showing Ps_3 botryoidal banded Fe-poor sphalerite and greenockite surrounding a pyrite crystal and an idiomorphic greenockite crystal

geothermal waters is thought to have been the main ore deposition mechanism. The maximum formation temperatures for these deposits exceed 350°C with a range between 200° and 400°C (Ohta 1995). The largest known Indium concentration reported is the Toyoha deposit, Japan, being one of the world's largest lead–zinc–copper–indium epithermal vein-type deposits, with an average indium grade of 140 ppm (Shwarz-Schampera and Herzig 2002). Indium concentrations in the polymetallic veins from Freiberg district, Germany show a wide range between 0.1 and 1,560 ppm In (Seifert and Sandmann 2006). These deposits have been defined as In-rich polymetallic vein-type deposits by Shwarz-Schampera and Herzig (2002).

Because of economic interest in Indium, it is important to examine new occurrences of this element. Hence, the aim of this study is to document the presence of an unusual mineralization style at the Pingüino deposit, and characterize the hydrothermal fluids that formed the indium-rich polymetallic mineralization from the Pingüino vein system in comparison with those responsible for classical epithermal low sulfidation mineralization elsewhere in the Deseado Massif.

Regional geological setting

Deseado Massif

The Deseado Massif (Fig. 1) is located in the centre of the Santa Cruz Province and belongs to the southern part of the Extra-Andean Patagonia in Argentina. The oldest rocks are Upper Precambrian slates and schists (La Modesta Formation) in the western sector and Upper Precambrian to Lower Paleozoic schists, gneisses, amphibolites and granitic intrusions (Río Deseado Complex), in the eastern sector. These basement rocks are covered by a Permian (Tres Cerros Group) to Triassic (El Tranquilo Group) continental sedimentary sequence that was deposited in a rift basin (Homovc and Constantini 2001). The earliest magmatic event is represented by Lower Jurassic diorites to granites, which intrude the Permian to Triassic sedimentary rocks. These intrusions (La Leona Complex), define a high-K calc-alkaline monzonite series interpreted as part of the Triassic–Early Jurassic Cordilleran interior belt that preceded widespread Middle to Upper Jurassic volcanism (Rapella and Pankhurst 1996). The intrusions are partially covered in the centre of the massif by Lower Jurassic volcaniclastic rocks (Roca Blanca Formation). Basaltic lava flows (El Piche Formation) overlie and are intercalated within the Lower Jurassic volcaniclastic rocks (Jovic 2010). These units are poorly represented in the Deseado Massif.

A Middle to Upper Jurassic, volcanic mega-event occurred in Patagonia, giving rise to the Chon Aike Large Igneous Province (Pankhurst et al. 1998; Pankhurst et al. 2000). In the Deseado Massif (Fig. 1), this event is represented by a volcanic suite that was named the Bahía Laura Volcanic Complex by Feruglio (1949) and Sruoga et al. (2008), and consists of the Bajo Pobre, Cerro León, Chon Aike and La Matilde Formations. The Bajo Pobre Formation is characterized by intermediate to basic calc-alkaline volcanic rocks that are mostly andesitic in composition (Panza and Haller 2002). These rocks are dominated by lavas, with subordinated ash flow tuffs and volcanic agglomerates. The Cerro León Formation is typified by subvolcanic intrusions (stocks, laccoliths, sills and dykes), which represent the feeder facies and intrusive equivalents of the Bajo Pobre Formation rocks (de Barrio et al. 1999; Jovic et al. 2008a). These rocks are best represented in the lower section of the Bahía Laura Volcanic Complex. The Chon Aike Formation is dominated by rhyolites, with minor dacites and trachydacites, of calc-alkaline, peraluminous and high-K signature. These rocks built an extensive rhyolitic plateau, dominated by vast volumes of pyroclastic material erupted as high fluidity ash flow tuffs. Pyroclastic rocks predominate, and ignimbrites represent the 90% of the outcrops, with subordinate amounts of intercalated lavas (Pankhurst et al. 1998; Panza and Haller 2002). Finally, the La Matilde Formation consists of a homogeneous sequence of ash fall tuffs and reworked volcaniclastic sediments formed in low energy fluvial and lacustrine settings, with minor intercalations of ash flow and fall tuff deposits (de Barrio et al. 1999). The Chon Aike and the La Matilde Formations are dominant in the Middle to Upper parts of the Bahía Laura Volcanic Complex sequence. Intricate stratigraphic relationships characterize the Bahía Laura Volcanic Complex, with multiple interdigitations of different lithologies (Echeveste et al. 2001; Guido et al. 2006; López 2006; Ruiz et al. 2008).

The Deseado Au–Ag metallogenical province

The Deseado Massif is an important Au–Ag producer with four mines (Cerro Vanguardia, Martha, San José and Manantial Espejo), and it is also the subject of intense exploration with more than 50 active projects. Numerous gold and silver low sulfidation epithermal deposits are spatially, temporally and genetically related with the Bahía Laura Volcanic Complex (Guido and Schalamuk 2003), leading Schalamuk et al. (1999) to define the Deseado Massif as an Au–Ag metallogenic province. Mineralization consists of quartz veins and veinlets, vein stockworks and hydrothermal breccias mainly hosted in Jurassic volcanic rocks. The dominant mineralization trend is NW, with subordinate NE and E-W structures. Gangue minerals are mostly of the silica group, mainly quartz with minor chalcedony and opal, and accompanied in some places by calcite, adularia, barite, fluorite and zeolites. The quartz textures are commonly massive, brecciated, crustiform and colloform banded with comb, cockade and lattice bladed textures. Metalliferous minerals are minor, representing commonly less than 10% in volume. They are mainly pyrite, native gold, electrum, argentite, native silver, Ag–sulfosalts, hematite, sphalerite, galena and chalcopyrite. The geochemical signature of the quartz-rich veins is typical of low sulfidation epithermal deposits. In addition to Au and Ag, they have elevated As, Sb, Hg, Mo, Pb, Zn, Mn and minor Cu (Echeveste 2005; Ruiz and Guido 2006). Hydrothermal alteration is restricted to the proximity of the veins and is represented by silicification, argillization (illite, smectite and kaolinite), sericitization (muscovite) and propylitization. The latter is better developed in the intermediate to basic lava flows. Silica and carbonate Jurassic hot spring deposits are widespread in association with the epithermal veins (Schalamuk et al. 1997). According to Guido and Schalamuk (2003), Schalamuk et al. (2005) and Jovic et al. (2009), the hydrothermal fluids responsible for the epithermal deposits of this region were neutral to alkaline H_2O+NaCl+KCl±$CaCl_2$±$FeCl_2$ solutions, with 0.18 to 8 eq.wt.% NaCl salinities and homogenization temperatures ranging from ~100°C to 320°C (for inclusions within quartz and adularia). Fluid $\delta^{18}O$ values between −6.4‰ and +5‰ for quartz suggest an important component of meteoric waters in the hydrothermal solutions, whereas fluid $\delta^{34}S_{CDT}$ values between −2.5‰ and +5‰ indicate a magmatic source for the sulfur. The Deseado Massif epithermal veins and hot spring deposits were formed during Middle to Upper Jurassic widespread extension, contemporaneous with the last stages of the Bahía Laura Volcanic Complex event (Arribas Jr et al. 1996; Schalamuk et al. 1997; Guido and Schalamuk 2003; Echavarría et al. 2005). The Cerro Vanguardia veins have ages between 152.9±2.75 Ma and 155.1±3.0 Ma (Ar/Ar in adularia; Sharpe et al. 2002) and the Martha deposit has an age of 154 Ma ($^{40}Ar/^{39}Ar$ in adularia; O'Leary and Sims 2009) similar to that of the nearby Manantial Espejo deposit (154±1 Ma, Ar/Ar in adularia; Wallier 2009). The San Jose deposit appears to be slightly younger with an age of 151.2 Ma ($^{40}Ar/^{39}Ar$ in adularia; Gutiérrez 2006).

Geological setting of Pingüino deposit

Middle to Upper Triassic continental sedimentary rocks of El Tranquilo Group (Jalfin and Herbst 1995; Fig. 2) are fine to coarse sandstones with volcanic components and rhythmic alternation of siltstones, mudstones, black shales and coal. Dioritic intrusive bodies, with associated mafic sills and dykes, assigned to the La Leona Complex of probably Lower Jurassic age (Jovic 2010) intrude the Triassic rocks. The Lower Jurassic Roca Blanca Formation (Herbst 1965) is composed of epiclastic and pyroclastic fine sandstones with conglomerate and tuffitic rocks, volcanic sandstones and some tuffaceous levels and minor ignimbrite deposits. Basaltic lava flows of the El Piche Formation (Jovic 2010) crop out in the northern part of the area, overlaying and intercalated within the volcaniclastic rocks of the Roca Blanca Formation. In the northwestern sector, the sequence is intruded by andesitic subvolcanic bodies, assigned to the Midlle Jurassic Cerro León Formation (Panza 1995). Regional structural dome (15 to 20 km in diameter) with radial faulting, NW fault systems and localized minor scale folding structures (<1 km) are recognized in the area. A deep intrusion (5–7 km deep) is responsible for the regional doming and the radial fracture system (Peñalva et al. 2008) and folded structures (domes, <1 km), represent local deformation associated with, generally not outcropping, subvolcanic bodies. These intrusions are located between −80 and −200 m depth and consist of dioritic (La Leona Complex) and minor to andesitic (Cerro Leon Formation) bodies, that have been confirmed by regional magnetometric surveys (Peñalva et al. 2008; Fig. 2b) and exploration drill holes (www.argentexmining.com and Cortiñas et al. 2005). The El Tranquilo Fault (N325°/70° NE) is the principal brittle structure, and is associated with secondary extensional faults to the east. The Pingüino vein district is composed of 74 linear km of veins that infill fault systems trending NW and ENE, hosted in Triassic continental sedimentary rocks and Lower Jurassic epiclastic and volcaniclastic rocks. These are spatially related (Fig. 2b) to the Lower Jurassic? dioritic intrusions (Jovic 2010) and form an extensional sinistral strike slip duplex system, within wich three main orientations can be recognized: namely the El Tranquilo (T) fault-vein system (N330°–N325°/80° NE), the Marta (M) fault-vein system (N300°–N310°), and the Kasia (K) fault-vein system (N260°–N250°). The T and M systems

Table 1 Summary geochemistry of polymetallic sulfide veins in the Pingüino deposit

Stage	Values	In (ppm)	Au (ppm)	Ag (ppm)	Cu (wt.%)	Pb (wt.%)	Zn (wt.%)	Sn (ppm)	Bi (ppm)	Cd (ppm)	As (wt.%)	Sb (ppm)	W (ppm)
Ps_1 (n=45)	Average	49.6	2.77	45.5	0.41	0.13	1.27	1,267	93.9	61.7	1.00	66.5	55.2
	Minimum	3.4	0.01	2.6	0.01	0.01	0.02	7	0.8	3.6	0.02	1.4	0.2
	Maximum	159	8.07	237	2.47	0.30	6.10	5,961	390	338	4.41	509	740
Ps_2 (n=100)	Average	161.8	0.74	156.3	0.14	3.65	10.81	153	5.3	848.5	0.40	87.0	2.4
	Minimum	5.25	0.10	14.5	0.01	0.16	0.08	23	0.1	6.0	0.07	5.0	0.1
	Maximum	1,184	1.34	684	5.99	19.30	32.95	564	30.1	14,900	1.28	634	25.2

comprise the main veins, where the major ore shoots are developed and named as follows: Marta Norte, Ana, Marta Noroeste, Savary, Marta Este, Marta Oeste, Marta Centro, Ivonne Norte, Marta Sur, Ivonne and Ivonne Sur. The K system also develops ore shoots when it lies close to the M veins system with Kasia, Kae and Kalia veins being the most important (Fig. 2a). The Pingüino deposit is characterized by the presence of two vein types, early polymetallic sulfide-rich veins and late quartz-rich veins. Polymetallic mineralization massive sulfide veins and breccias up to 13 m thick have Sn, W, Cu, Au, As, Bi, Zn, Pb, Ag, In, Cd and Sb geochemical signature (Table 1). Quartz-rich veins represented by breccias and veins have a maximum thickness of 20 m and are composed of quartz, carbonates, clays and minor sulfides with colloform and crustiform banding, comb, cockade and minor lattice bladed textures. These have comparatively high Ag, Au values and Ag/Au ratios. The late Ag–Au–quartz-rich veins crosscut the early polymetallic sulfide-rich veins implying the coincidence of the two different mineralization styles in the same fault system. The quartz-rich veins have similar characteristics to the typical low sulfidation type mineralization from the Deseado Massif (Jovic et al. 2008b; Jovic 2010) and are not discussed further here.

Analytical methods

To determine the mineralization stages and ore mineralogy of the polymetallic mineralization detailed microscopy studies and back-scattered scanning electron microscope imaging of minerals in polished thin sections were carried out at the Departament de Cristalografía, Mineralogía y Dipòsits Minerals at the University of Barcelona, Spain (Jovic et al. 2005; Crespi et al. 2006).

Representative samples from the different mineralizing stages were analysed at Acme Analytical Laboratories in Vancouver, Canada (http://acmelab.com/). Sample splits of 0.5 g were leached in 3 ml of hot (95°C) Aqua Regia, HCl–HNO_3–H_2O, and analysed by inductively coupled plasma-mass spectrometry for precious and base metals.

Microscopy and microthermometric characterization of fluid inclusions in quartz were done using a USGS Fluid inclusion heating-freezing system stage attached to a Leica DMR-XP microscope, and a Chaixmeca heating-freezing stage fitted to a Leitz Ortholux microscope. An infrared (IR) microscopy system in the NIR (near infrared, up to 10 μm) and short wavelength infrared (up to 1.4 μm) was used for microscopy and microthermometric studies of fluid inclusions in opaque (Fe-rich sphalerites (Ríos et al. 2006; Jovic et al. 2007).

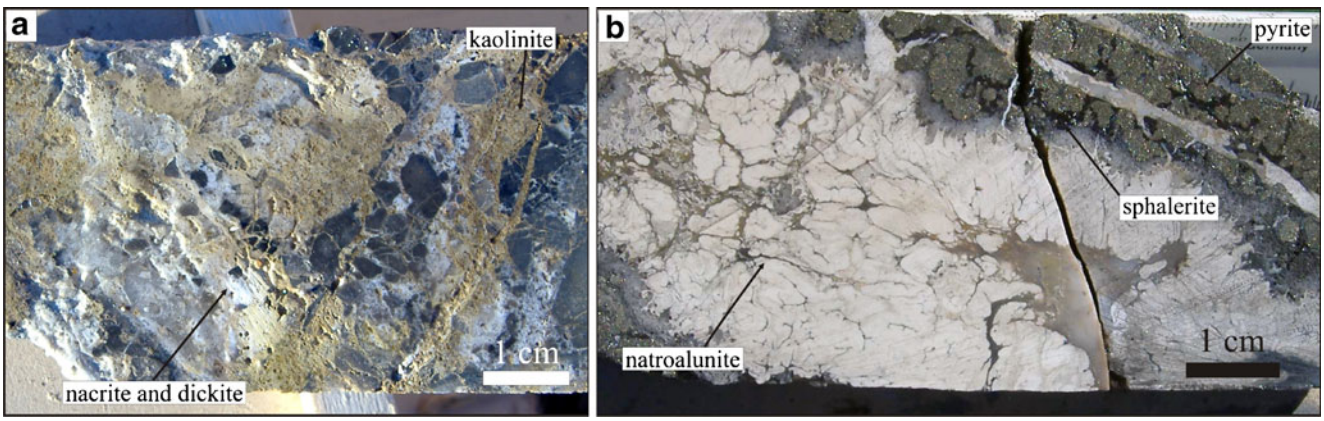

Fig. 4 Hydrothermal alteration associated with polymetallic mineralization represented by dickite, nacrite and kaolinite (**a**) and natroalunite (**b**)

The salinity was calculated from the Tm_{ice} values using the method of Bodnar and Vityk (1994). The fluid inclusion microthermometric studies were done in quartz and sphalerites. All the samples studied contain two-phase (L+V) aqueous fluid inclusions. Primary fluid inclusions were selected and studied on the basis of their occurrence in growth zones and their morphology. The fluid inclusions are mostly 10 to 17 μm in size with a maximum of 100 μm. Ice-melting temperatures ranged between −7.4°C and −27.1°C for most samples.

Preliminary stable isotope studies on sulfur ($^{34}S/^{32}S$) were carried out in the Stable Isotopes Laboratory of the University of Salamanca, Spain, using the technique described by Robinson and Kusakabe (1975). The sulfur dioxide produced was analysed online by a VG SIRA 2 mass spectrometer. All sulfur isotope results are expressed in conventional delta ($\delta^{34}S$) notation. Reproducibility based on complete duplicate analyses (including combustion) was better than 0.3‰.

Lead isotopic analyses were carried out on whole rock and ore minerals at the Geochronological Research Center, University of São Paulo. Samples used for isotopic analyses were selected on the basis of petrographic and mineralogical characteristics derived using thin and polished sections and back-scattered scanning electron microscope imaging. The Pb isotopic analyses included washing samples with $HCl+HNO_3$ and dissolution with HCl in Parr type bombs. The Pb was separated using HCl and HBr in an AG1-X8 (200–400#) column. The procedural blank for Pb was 70 pg. Pb isotope ratios were corrected relative to the values of the NBS981 standard by 1.0024 for $^{206}Pb/^{204}Pb$, 1.0038 for $^{207}Pb/^{204}Pb$, and 1.0051 for $^{208}Pb/^{204}Pb$. The analytical errors for these isotopic ratios were 0.15% to 0.48%, 0.13% to 1.07% and 0.104% to 0.45%, respectively. Lead isotopic analyses were determined on a multicollector VG354 Micromass mass spectrometer

In-bearing polymetallic mineralization

Mineralization stages and ore mineralogy

The sulfide-rich veins are poorly exposed at surface and are characterized by the presence of gossans with remnants of breccias of quartz matrix and oxidized sulfide clasts. The mineralogy of the gossans is characterized by goethite, reddish kaolinite (Fig. 3a, b), supergene Pb minerals (plumbojarosite ($PbFe_6(SO_4)O_{12}$) and plumbonacrite ($Pb_{10}(CO_3)_6O(OH)_6$)). Soil and trench geochemistry shows high contents of Fe, Pb, Cd, In and Bi, Cu, Au, As and Sb. The oxidation zone varies between 30 to 60 m in depth (Jovic et al. 2009).

Hypogene polymetallic mineralization is characterized by massive and banded sulfide veins and breccias (Fig. 3)

Table 2 Microthermometric data from fluid inclusions of polymetallic veins from Pingüino deposit

Mineralization stage	Vein	Drill hole	Depth (metres)	Mineral	Inclusion type	Th range (°C)	Tm_{ice} range (°C)	Th average (°C)	Salinity range (eq.wt.% NaCl)	Average salinity (eq.wt.% NaCl)	Number of measurements
Ps_1	Ivonne	102	53.3–70.5	Qtz	Primary	308.2–327	−1.7 to −2.7	319.3	2.90–4.49	3.91	8
Ps_2	Marta Centro	53	54.2–81	Spl	Primary	255–312.4	−2.6 to −5.7	273.5	4.34–8.81	6.51	14

Th homogenization temperature, Tm_{ice} final melting temperature of ice

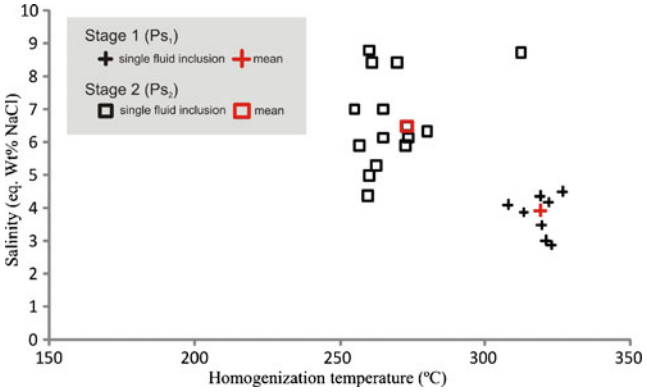

Fig. 5 Salinity versus homogenization temperature of fluid inclusions in quartz and sphalerite from polymetallic mineralization of Pingüino deposit

up to 13 m thick, with high grade ore shoots, developed between 30/60 to 400 m depth (www.argentexmining.com). The ore geochemistry indicates the presence of high concentrations of Cu, Au, As, Sn, W, Bi, Zn, Pb, Ag, In, Cd and Sb in the sulfide-rich veins (Table 1).

The polymetallic mineralization of the Pingüino deposit developed in three main stages, an early Au, Cu, Sn, In, Bi, As and W (Table 1) stage (Ps_1; Fig. 3c, d) which is characterized by a complex paragenesis composed mainly of idiomorphic pyrite crystals, rhombic zoned arsenopyrite crystals up to 1 cm and hypidiomorphic chalcopyrite crystals between 10 μm and 2 mm. Minor small (<50 μm) crystals of pyrrhotite and marcasite are present associated with pyrite and arsenopyrite. Cassiterite is present as allotriomorphic crystals between 5 and 20 μm and idiomorphic crystals up 200 μm, that fill fractures and are associated with radially aggregated and idiomorphic hübnerite ($MnWO_4$) crystals (<1 mm). Ferrokësterite ($Cu_2(Fe,Zn)SnS_4$) and stannite (Cu_2FeSnS_4) replace cassiterite. Very fine grained (<50 μm) acicular and prismatic Ag–Bi, Ag–Pb–Bi, Pb–Bi sulfosalts including aramayoite ($Ag(Sb,Bi)S_2$), owyheeite ($Pb_7Ag_2(Sb,Bi)_8S_{20}$), ourayite ($Pb_4Ag_3Bi_5S_{13}$), giesenite ($Cu_2Ag_{26}(Sb,Bi)_{20}S_{57}$) and izoklakeite ($Pb_{27}(Cu,Fe)_2(Sb,Bi)_{19}S_{57}$) are present late in this stage. Minor amounts of sphalerite, galena, bournonite ($PbCuSbS_3$), argentotennantite and quartz are also recognized. The indium is present in Sn-rich minerals, as exsolutions at submicroscopic scale (Jovic 2010), mainly in ferrokësterite where the highest content occurs (between 0.04 and 3.02 wt.% with an average of 0.51 wt.%, n=52), and secondarily in the cassiterite where the indium values ranged between 0.14 and 0.36 wt.% with a mean of 0.22%, n=16 (Jovic 2010). This stage is best represented in the Ivonne vein (Jovic et al. 2005; Crespi et al. 2006).

The second stage paragenesis (Ps_2; Fig. 3e, f) is high in Zn, Pb, In, Ag, Cd and Sb (Table 1). Ps_1 minerals were replaced or brecciated mainly by banded sphalerite and galena (Ps_2). The sphalerite is the most abundant mineral; is black in hand specimens and crystals are allotriomorphic to idiomorphic up to 2 cm. Galena is very abundant and is present in irregular masses or idiomorphic crystals up to few cm, intergrowth with the sphalerite. Hypidiomorphic tetrahedrite and freibergite crystals between 100 and 500 μm and allotriomorphic argentotennantite (<20 μm) grains and Pb-Ag sulfosalts grains (<20 μm) are present in this stage. Late and minor enargite grains (<50 μm) are present in galena cleavage planes or as irregular masses related to freibergite. The indium is present in Fe-rich sphalerites with values ranging between 0.01 and 2.57 wt.% and a mean of 0.47%, n=10 (Jovic 2010). The presence of indium in the sphalerite is related to structural substitution of In, Cu and minor Cd, with a coupled substitution of 2 (Zn,Fe) for CuIn (Jovic et al. 2009). The Ps_2 stage is best developed in the Marta Centro vein (Jovic et al. 2005; Crespi et al. 2006).

A third mineralization stage (Ps_3; Fig. 3g and h) was recognized only by microscopy and is interpreted to represent remobilization from Ps_1 and Ps_2 (Jovic 2010). It is characterized by idiomorphic greenockite crystals (<25 μm) and botryoidal banded Fe-poor sphalerite and greenockite surrounding pyrite, stannite and also greenockite crystals. This stage is represented in Ivonne and Marta Centro veins (Jovic et al. 2005; Jovic 2010).

Hydrothermal alteration

The hydrothermal alteration associated with the polymetallic mineralization is characterized by advanced argillic alteration and silicification within the immediate vein zone, and sericitic alteration enveloping the vein zone. Pervasive silicification is characterized by varying amounts of quartz and pyrite that rarely penetrates more than 1 to 2 m into the country rock. The advanced argillic alteration is characterized by kaolinite, dickite and nacrite ($Al_2Si_2O_5(OH)_4$) (Fig. 4a), and includes natroalunite ($NaAl_3(SO_4)_2(OH)_6$) (Fig. 4b) and kalinite ($KAl(SO_4)\cdot 11(H_2O)$). These minerals occur as pervasive replacement and as veinlets, and are clearly related to the hypogene polymetallic vein mineralization. Sericitic alteration occurs for tens of metres into the country rocks, mainly in the volcaniclastic rocks and sandstones. Potassic (boitite) and propylitic alteration (epidote, Fe chlorite, calcite and pyrite) are localized around diorite intrusions, but their relationship to the veins is not clear.

Geochemistry, fluid inclusion and isotopic studies

Geochemical analysis (Table 1) shows that Ps_1 (n=45), concentrations of indium up to 159.4 ppm correlate with

Sn (r=0.77), Sb (r=0.77) and Ag (r=0.70). The highest values of Indium are present in Ps_2 samples (up to 1,184 ppm) and display a high correlation with Zn (r=0.77; n=100) and Cd (r=0.80) indicating an important relationship between indium, zinc and cadmium (Jovic et al. 2009).

The fluid inclusion microthermometric results are given in Table 2 and Fig. 5. Primary fluid inclusions in quartz grains were studied from polymetallic stage Ps_1. The homogenization temperatures (Th) of the inclusions ranged between 308 and 327°C with a mean of 319°C. The salinity varies between 2.1 and 4.5 eq.wt.% NaCl with an average of 3.91. Under transmitted light, Ps_2 Fe-rich sphalerites have a pale grey colour and the fluid inclusions and other features are opaque or indistinguishable. IR microscopy allowed the observation of growth lines and solid and fluid inclusions. Under IR light it is possible to observe large primary (L+V) aqueous fluid inclusions (up to 100 μm) with different shapes (tube like and spherical). Ice melting was measured between −2.6°C and −5.7°C, which indicates low to moderate salinity (4.34 to 8.81 with a mean of 6.53 eq.wt.% NaCl) and homogenization temperatures between 255°C and 312°C, with a mean of 273°C.

Sulfur isotopic analyses were undertaken of pyrite, arsenopyrite and chalcopyrite from Ps_1, and sphalerite and galena from Ps_2 (Table 3). The $\delta^{34}S$ values of sulfide minerals from the ore are remarkably homogeneous and range between +0.8‰ and +3.6‰, with mean values of +1.5‰ for the P_{S1} and +2.5‰ for the Ps_2.

Pyrite, arsenopyrite, sphalerite and galena from the polymetallic mineralization have similar $^{206}Pb/^{204}Pb$, $^{207}Pb/^{204}Pb$ and $^{208}Pb/^{204}Pb$ ratios of 17.379 to 18.502, 15.588 to 15.730 and 38.234 to 38.756, respectively (Table 3). The results from sulfides and magmatic rocks were plotted on conventional $^{207}Pb/^{204}Pb$ vs. $^{206}Pb/^{204}Pb$ and $^{208}Pb/^{204}Pb$ vs. $^{206}Pb/^{204}Pb$ diagrams (Fig. 6). Pb isotopic ratios for the sulfides and magmatic rocks from Pingüino area fall on or close to the crustal growth curve of Zartman and Doe

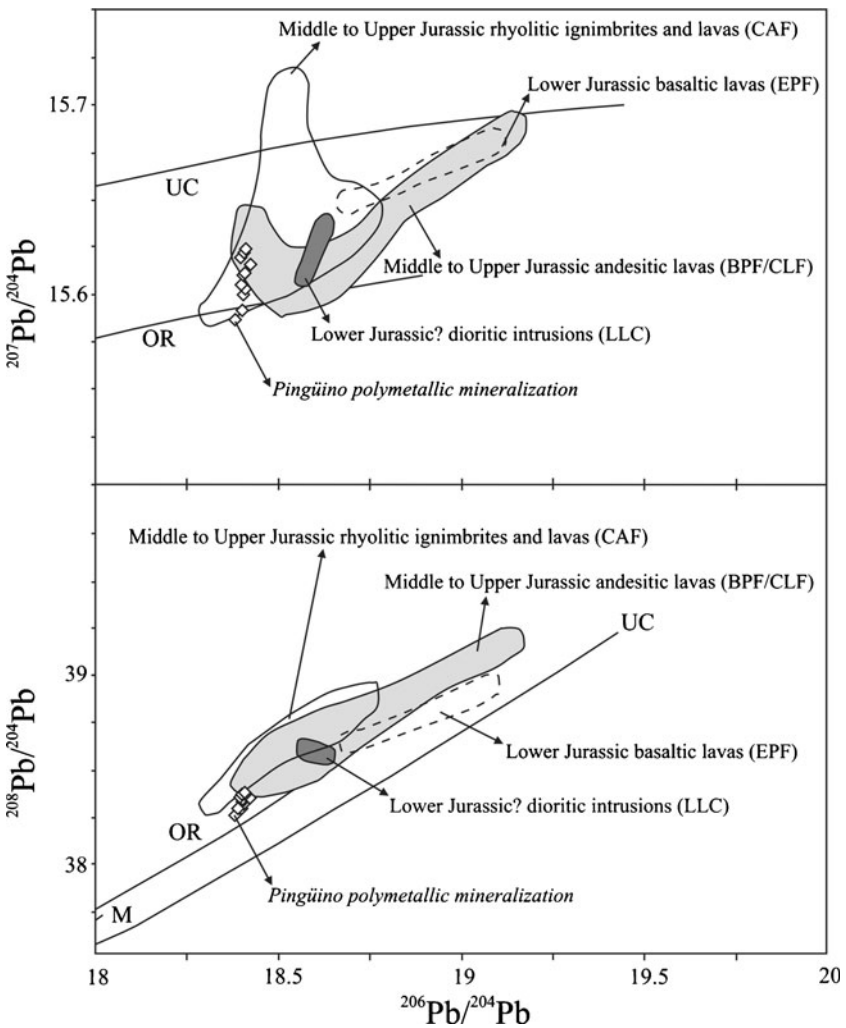

Fig. 6 Lead isotope compositions of Jurassic magmatic rocks and sulfide minerals from the polymetallic mineralization. *CAF* Chon Aike Formation (data from López 2006; Moreira 2005), *BPF/CLF* Bajo Pobre and Cerro León Formations (data from this study, López 2006; Moreira 2005), *LLC* La Leona Complex (data from this study), *EPF* El Piche Formation (data from this study). The mantle (*M*), orogen (*OR*) and upper-crust (*UC*) evolution curves are from Zartman and Doe (1981)

Table 3 S and Pb isotopic compositions of rocks and polymetallic mineralization from Pingüino deposit

Sample no.	Lithology/Mineral	$\delta^{34}S$ (‰)	$^{206}Pb/^{204}Pb$ (±2 sigma)	$^{207}Pb/^{204}Pb$ (±2 sigma)	$^{208}Pb/^{204}Pb$ (±2 sigma)
5739	Dioritic intrusion (whole rock)	–	18.628 (0.009)	15.640 (0.009)	38.543 (0.007)
6101	Dioritic intrusion (whole rock)	–	18.568 (0.005)	15.608 (0.005)	38.585 (0.005)
5794	Basaltic lava (whole rock)	–	19.081 (0.004)	15.682 (0.005)	38.917 (0.005)
4203	Basaltic lava (whole rock)	–	18.684 (0.005)	15.652 (0.004)	38.617 (0.004)
4404	Andesitic porphyry (whole rock)	–	18.606 (0.004)	15.614 (0.005)	38.541 (0.004)
6035	Andesitic porphyry (whole rock)	–	18.623 (0.004)	15.621 (0.004)	38.516 (0.004)
4205	Andesitic lava (whole rock)	–	18.534 (0.005)	15.617 (0.005)	38.475 (0.005)
5615	Andesitic lava (whole rock)	–	18.496 (0.006)	15.603 (0.006)	38.394 (0.004)
1718a	Pyrite	1.32	18.408 (0.007)	15.625 (0.007)	38.341 (0.007)
7152	Pyrite	2.16	18.398 (0.010)	15.593 (0.011)	38.269 (0.011)
1600a	Pyrite	1.56	18.502 (0.023)	15.730 (0.032)	38.756 (0.041)
1563	Pyrite	2.36	18.476 (0.165)	15.704 (0.161)	38.643 (0.201)
1718b	Pyrite	2.36	18.400 (0.008)	15.601 (0.009)	38.302 (0.008)
7065	Arsenopyrite	1.56	18.395 (0.009)	15.606 (0.009)	38.319 (0.010)
1586a	Arsenopyrite	0.76	18.402 (0.024)	15.612 (0.024)	38.318 (0.025)
1586b	Quartz	–	18.404 (0.008)	15.604 (0.008)	38.295 (0.008)
7280a	Sphalerite	1.56	18.406 (0.010)	15.622 (0.009)	38.335 (0.009)
7283a	Sphalerite	1.86	18.407 (0.024)	15.613 (0.024)	38.313 (0.025)
7283b	Galena	3.61	18.397 (0.028)	15.620 (0.029)	38.339 (0.030)
7280b	Galena	3.61	18.379 (0.007)	15.588 (0.007)	38.234 (0.008)
1600b	Arsenopyrite	1.06	–	–	–
264a	Arsenopyrite	1.16	–	–	–
264b	Chalcopyrite	2.84	–	–	–
7152	Chalcopyrite	1.54	–	–	–
1292a	Sphalerite	1.36	–	–	–
1292b	Galena	3.01	–	–	–

(1981), indicating that the Pb reservoirs for both became from a crustal source. Intermediate and basic magmatic rocks from Pingüino deposit have similar Pb isotopic compositions of the sulfides to polymetallic mineralization.

Discussion

Indium-bearing polymetallic vein-type deposits comprise a very heterogeneous group, showing transitions to granite-related vein-stockwork and porphyry tin–tungsten deposits and to base metal-rich epithermal-style mineralization. They are linked genetically to postcollisional and Proterozoic to Tertiary subduction-related metallogenic processes. Indium mineralization affected a variety of, clastic metasedimentary and metavolcanic, rhyolitic-dacitic-andesitic host rocks. Close associations with subaerial porphyritic rocks imply genetic relationships to subvolcanic intrusions. In addition, indium-bearing veins display a heterogeneous source of mineralizing fluids ranging from basinal brines to fluids with significant contributions of magmatic volatiles (Schwarz-Schampera and Herzig 2002).

On the basis of the paragenetic study, ore and alteration mineralogy, geochemical signature, fluid inclusion and isotopic data, it is clear that the polymetallic mineralization at the Pingüino deposit represents a different deposit type compared with the classical low sulfidation epithermal mineralization recognized in the Deseado Massif (Table 4).

Indium concentration in the polymetallic mineralization from Pingüino deposit is similar to those reported for the polymetallic veins of the Freiberg district and Toyoha mine (Ohta 1995; Schwarz-Schampera and Herzig 2002).

Indium was mainly concentrated during the Ps_2 mineralization stage, predominantly within Fe-rich sphalerites, although significative In enrichment is also present in Ps_1 mineralization stage Sn-minerals (ferrokesterite and cassiterite).

Advanced argillic alteration is commonly associated with high sulfidation epithermal deposits (Simmons et al. 2005) but is also with some polymetallic veins and cordilleran epithermal deposits (Bendezú and Fontboté 2009). The acid solutions responsible for the characteristic assemblage (quartz+alunite ±pyrophyllite±dickite±kaolinite; Simmons et al. 2005) can be traced directly to shallow intrusions that exsolve a fluid in much the same manner as is inferred for the development of

Table 4 Deseado Massif Au–Ag mineralization and Pingüino polymetallic mineralization characteristics

	Deseado Massif Au–Ag mineralization	Pingüino polymetallic mineralization
Deposit style	Mainly NW strike structurally controlled quartz chalcedony veins and breccias	NW and ENE strike structurally controlled sulfide veins and breccias
Host rock	Middle to Upper Jurassic volcanism and minor older units (Pz, Pm)	Triassic to Lower Jurassic sedimentary and volcaniclastic rocks
Textures	Massive, brecciate, crustiform and colloform banding with comb, cockade and lattice bladed texture	Massive, brecciate and banded
Ore mineralogy	Pyrite, native gold and silver, electrum, argentite, Ag–sulphosalts, hematite, sphalerite, galena and chalcopyrite	Pyrite, arsenopyrite, sphalerite, galena, chalcopyrite, cassiterite, stannite, ferrokësterite, wolframite, Ag–Bi–Pb–sulphosalts, tetrahedrite and freibergite
		Pb–Ag–sulphosalts, bournonite, argentotenantite, enargite and greenockite
Gangue mineralogy	Quartz, chalcedony, adularia and calcite	Quartz
Hydrothermal alteration	Silicification, argillization (illite, smectite and kaolinite), sericitization (sericite) and propylitization	Advanced argillization (kaolinite, dickite, nacrite, natroalunite, kalinite), silicification and sericitization (sericite)
Metals	Au–Ag (As, Sb, Hg, Mo, Pb, Zn, Mn and Cu)	Zn, Pb, Ag, In (Cu, Au, As, Sn, W, Bi, Cd and Sb)
% sulfides	<10% in volume	>90% in volume
Homogenization temperatures	<100° to 320°C	255° to 327°C
Salinities	0.18 to 8 eq.wt.% NaCl (quartz and adularia)	2.09 and 8.81 eq.wt.% NaCl (quartz and sphalerite)
S isotopes	$\delta^{34}S_{CDT}$ −2.5‰ to +5‰ (sulfides)	$\delta^{34}S_{CDT}$ +0.76 to +3.61 (sulfides)
Pb isotopes	$^{206}Pb/^{204}Pb$: 18,307 to 18,720	$^{206}Pb/^{204}Pb$: 18,379 to 18,502 $^{207}Pb/^{204}Pb$:15,588 to 15,730
	$^{207}Pb/^{204}Pb$: 15,590 to 15,953	
	$^{208}Pb/^{204}Pb$: 38,290 to 39,527	$^{208}Pb/^{204}Pb$: 38,234 to 38,756
O isotopes	$\delta^{18}O_{fluids}$ −6.4‰ to +5‰ (quartz)	–
Age	~154 Ma (adularia)	Lower Jurassic?
Possible source rocks	Middle to Upper Jurassic volcanism (Bahía Laura Volcanic Complex)	Lower Jurassic?−intermediate magmatism (La Leona Complex)

porphyry copper deposits (Hedenquist et al. 1998; Heinrich et al. 2004). For fluids that form quartz+alunite±pyrophyllite ±dickite±kaolinite assemblage, moderate-to high-salinity fluid inclusions reflect the history of fluid exsolution during crystallization of underlying magmas (e.g., Hedenquist et al. 1998; Heinrich et al. 2004; Heinrich 2005), although most salinities are low, <5 wt.% NaCl equiv (Simmons et al. 2005). In the case of the Pingüino deposit, the polymetallic mineralization is spatially related to intrusions and is inferred to have formed from moderate salinity fluids (2–9 eq.wt.% NaCl). The advanced argillic alteration is therefore inferred to be related to acidic magmatic hydrothermal solutions exsolved from the dioritic intrusions.

Sulfur isotopes (+0.8‰ to +3.6‰) indicate a magmatic source for the polymetallic mineralization, specifically related to basic to intermediate magmatism (cf. Ohmoto and Rye 1979; Hoefs 1987; Ohmoto and Goldhaber 1997; Recio 2000). In the Pingüino area the basic-intermediate magmatism is represented by dioritic intrusions of the La Leona Complex, basaltic lavas in the El Piche Formation and also the Middle Jurassic andesites from Cerro León and Bajo Pobre Formations.

Pb isotope ratios for the sulfides and magmatic rocks fall on, or close to the crustal growth curve of Zartman and Doe (1981), consistent with the possibility that the Pb reservoirs for both had the same crustal source.

Regional magnetometric surveys (Fig. 2b; Peñalva et al. 2008) and exploration drill holes (www.argentexmining.com and Cortiñas et al. 2005) clearly shows a spatial relationship between the sulfide veins and non-outcropping dioritic intrusions. The La Leona Complex (dioritic intrusions) could be part of the Triassic–Early Jurassic Cordilleran interior belt related to east-dipping and oblique subduction at the margin of Gondwana (Rapella and Pankhurst 1996). The In-bearing Pingüino deposit could therefore represent a distinctive product of early Mesozoic subduction in the Deseado Massif.

Conclusions

1. Polymetallic mineralization from Pingüino deposit has high In values (up to 1,184 ppm), with geochemical, mineralogical and metallogeneic similarities to important Indium-bearing polymetallic deposits from Japan (e.g. Toyoha deposit), Bolivia (e.g. Bolivar deposit) and Germany (Freiberg district).
2. The highest indium values were achieved during the Ps_2 mineralization stage, related mainly with Fe-rich

sphalerites, although significative In anomalies are also present in Ps_1 mineralization stage associated with Sn-minerals (ferrokesterite and cassiterite).

3. Spatial relationships, hydrothermal alteration styles, S and Pb isotopic data suggest that the possibly Lower Jurassic dioritic intrusions of the La Leona Complex could have been the source of metals and hydrothermal fluids for the polymetallic mineralization.
4. Mineralization paragenesis, the association with adavanced argillic alteration, geochemical signatures, fluid inclusion data and isotopic data, confirm that the polymetallic mineralization of the Pingüino deposit represents a distinct deposit type as compared to classical Middle to Upper Jurassic epithermal low sulfidation mineralization in the Deseado Massif.

Acknowledgements This contribution forms part of the senior author's Ph.D. thesis at the Universidad Nacional de La Plata-CONICET, Argentina. We thank Ken Hicks and the Argentex Mining Corporation for their constant support. We also appreciate the support, discussions and constructive suggestions given by Gerardo Paéz and Remigio Ruiz. Patrick Williams, Noel White, Thomas Bissig, Rolf Romer and an anonymous reviewer are thanked for very constructive reviews.

References

Arribas A Jr, Schalamuk IB, de Barrio R, Fernández R, Itaya T (1996) Edades Radimétricas de Mineralizaciones Epitermales Auríferas del Macizo del Deseado, Provincia de Santa Cruz, Argentina. IGCP Project 342: age and isotopes of South American Ores. ACTAS XXXIX Congresso Brasileiro de Geología 6:254–257.

Bendezú R, Fontboté L (2009) Cordilleran epithermal Cu–Zn–Pb–(Au–Ag) mineralization in the Colquijirca district, Central Peru: deposit-scale mineralogical patterns. Econ Geol 104:905–944

Benzaazoua M, Marion P, Pinto A, Migeon H, Wagner FE (2003) Tin and indium mineralogy within selected samples from the Neves Corvo ore deposit (Portugal): a multidisciplinary study. Miner Eng 16:1291–1302

Binns RA, Scott SD (1993) Actively forming polymetallic sulfide deposits associated with felsic volcanic rocks in the eastern Manus back-arc basin, Papua New Guinea. Econ Geol 88 (8):226–236

Bodnar RJ, Vityk MO (1994) Interpretation of microthermometric data for H_2O–NaCl fluid inclusions. In: De Vivo B, Frezzotti ML (eds) Fluid inclusions in minerals, methods and applications. Virginia Tech, Blacksburg, pp 117–130

Boorman RS, Abbott D (1967) Indium in co-existing minerals from the Mount Pleasant tin deposit. Can Mineral 9(2):166–179

Burke EAJ, Kieft C (1980) Roquesite and copper- indium -bearing sphalerite from Långban, Bergslagen, Sweden. Can Mineral 18 (3):361–363

Carrillo-Rosúa J, Morales-Ruano S, Fenoll P (2008) Textural and chemical features of sphalerite from the Palai-Islica deposit (SE Spain): implications for ore genesis and color. Neues Jahrb Mineral 185(1):63–78

Cortiñas J, Homovc J, Lucero M, Gobbo E, Laffitte G, Viera A (2005) In: Chebli AG, Cortiñas JS, Spalletti LA, Legarreta L, Vallejo EL (eds) Las cuencas de la región del Deseado, provincia de Santa Cruz. Frontera exploratotia de la argentina, 1°th edn. Instituto Argentino del Petróleo y del Gas, Buenos Aires, pp 289–305

Crespi A, Jovic SM, Guido DM, Proenza J, Melgarejo JC, Schalammuk IB (2006) El prospecto Cerro León, Macizo del Deseado, Patagonia, Argentina: Un depósito de Ag-Sn. Macla 6:143–145

de Barrio R, Panza JL, Nullo F (1999) Jurásico y Cretácico del Macizo del Deseado, provincia de Santa Cruz. In: Caminos, R. (ed.), Geología Argentina 29 (17): 511–527

Echavarría LE, Schalamuk IB, Etcheverry RO (2005) Geologic and tectonic setting of Deseado Massif epithermal deposits, Argentina, based on El Dorado–Monserrat. J S Am Earth Sci 19:415–432

Echeveste H (2005) Metalogénesis del distrito argentoaurífero Manantial Espejo, Macizo del Deseado. Provincia de Santa Cruz. Ph.D. thesis, University of La Plata. p. 200

Echeveste H, Fernandez R, Bellieni G, Tessone M, Llambias E, Schalamuk I, Piccirillo E, Demin A (2001) Relaciones entre las Formaciones Bajo Pobre y Chon Aike (Jurásico medio a superior) en el área de Estancia El Fénix–Cerro Huemul, zona centro-occidental del Macizo del Deseado, provincia de Santa Cruz. Rev Asoc Geol Argent 56(4):548–558

Feruglio E (1949) Descripción geológica de la Patagonia. 3 Volumes, Dirección Nacional de Yacimientos Petrolíferos Fiscales, Buenos Aires.

Fouquet Y, Wafik A, Cambon P, Mevel C, Meyer G, Gente P (1993) Tectonic setting and mineralogical and geochemical zonation in the Snake Pit sulfide deposit (Mid-Atlantic Ridge at 23°N). Econ Geol 88(8):2018–2036

Gorelikova N, Tolosana-Delgado R, Pawlowsky-Glahn V, Khanchuk A, Gonevchuk V (2006) Discriminating geodynamical regimes of tin ore formation using trace element composition of cassiterite: the Sikhote' Alin case (Far Eastern Russia). Geol Soc Spec Publ 264:43–57

Guido DM, Schalamuk IB (2003) Genesis and exploration potential of epithermal deposits from the Deseado Massif, Argentinean Patagonia. In: Eliopoulos et al (eds) Mineral exploration and sustainable development. Balkema, Rotterdam, pp 493–496

Guido DM, Jovic SM, Schalamuk IB (2005) A new metallogenic association (Sn–Cd–In-Zn–Ag–Au) in the Deseado auroargentiferous province, Deseado Massif, Patagonia, Argentina. Mineral deposit research: meeting the global challenge. Springer Berlin Heilderberg New York 2:965–968

Guido DM, Escayola M, de Barrio RE, Schalamuk IB, Franz G (2006) La Formación Bajo Pobre (Jurásico) en el este del Macizo del Deseado, Patagonia Argentina: Vinculación con el Grupo Bahía Laura. Rev Asoc Geol Argentina 61(2):187–196

Gutiérrez R (2006) Geology of the Huevos Verdes silver-gold vein system, San Jóse District, Deseado Massif, Patagonia, Argentina. M.Sc. thesis, Colorado School of Mines. p. 166

Hedenquist JW, Arribas A Jr, Reynolds TJ (1998) Evolution of an intrusion-centered hydrothermal system: far Southeast-Lepanto porphyry and epithermal Cu–Au deposits, Philippines. Econ Geol 93:373–405

Heinrich CA (2005) The physical and chemical evolution of low-salinity magmatic fluids at the porphyry to epithermal transition: a thermodynamic study. Miner Deposita 39:864–889

Heinrich CA, Driesner ST, Seward TM (2004) Magmatic vapor contraction and the transport of gold from the porphyry environment to epithermal ore deposits. Geology 32:821–824

Herbst R (1965) La flora fósil de la Formación Roca Blanca, provincia de Santa Cruz, Patagonia, con consideraciones geológicas y estratigráficas. Opera Lilloana 12:1–102

Hoefs J (1987) Stable isotope geochemistry. Springer, Berlin, p 237

Homovc J, Constantini L (2001) Hydrocarbon exploration potential within interplate shear-related depocenters: Deseado and San Julián basins, Southern Argentina. Am Assoc Pet Geol 85 (10):1795–1816

Huston DL, Sie SH, Suter GF, Cooke DR, Both RA (1995) Trace elements in sulfide minerals from eastern Australian volcanic-hosted massive sulfide deposits: part I. Protein microprobe analyses of pyrite, chalcopyrite and sphalerite, and part II. Selenium levels in pyrite: comparison with S values and implications for the source of sulfur in volcanogenic hydrothermal systems. Econ Geol 90(5):1167–1196

Ishihara S, Hoshino K, Murakami H, Endo Y (2006) Resource evaluation and some genetic aspects of indium in the Japanese ore deposits. Resour Geol 56(3):347–364

Jalfin G, Herbst R (1995) La Flora triásica del Grupo El Tranquilo, provincia de Santa Cruz (Patagonia). Estratigrafía. Ameghiniana 32(3):211–229

Jovic SM (2010) Geología y Metalogénesis de las mineralizaciones polimetálicas del área El Tranquilo (Cerro León), sector central del Macizo del Deseado, Provincia de Santa Cruz. (1ra ed.) Editorial de la Universidad de La Plata (EDULP), La Plata. p. 278

Jovic SM, Guido DM, Schalamuk IB, Melgarejo JC, Proenza J (2005) Mineralogía de veta Ivonne, deposito Cerro León: ¿Paragénesis de alta temperatura en la Provincia Auroargentifera del Deseado? XVI Congreso Geológico Argentino Actas 2:257–262

Jovic SM, Guido DM, Schalamuk IB, Ríos FJ, Fuzikawa K, Alves J (2007) NIR/SWIR microscopy and microthermometry of fluid inclusions from Fe-rich sphalerites, Cerro León (Zn-Pb-Ag-In-Au) polymetallic vein deposit, Deseado Massif, Patagonia, Argentina. Mineral Exploration and Research: Digging Deeper. Irish Association for Economic Geology 1:757–760

Jovic SM, Jovic NR, Guido DM, Schalamuk IB (2008a) Caracterización de cuerpos intrusivos de la formación Cerro León en el área del Anticlinal el Tranquilo, Macizo del Deseado, Santa Cruz. XVII Congreso Geológico Argentino. Actas (2): 851–852

Jovic SM, Lorenti Borda MP, Guido DM, Schalamuk IB (2008b) Primera mención de rodocrosita en vetas epitermales del Macizo del Deseado. 9°Congreso de Mineralogía y Metalogenia. XVII Congreso Geológico Argentino 1: 43–46.

Jovic SM, Liñan P, Guido DM, Paéz GN, Ruiz R, Schalamuk IB (2009) Metals distribution and correlations in polymetallic veins from Pingüino Indium-bearing deposit, Deseado Massif, Patagonia, Argentina. In: 24th International Applied Geochemistry Symposium, Fredericton, New Brunswick, Canadá, vol. 1. pp. 501–504

Kieft K, Damman AH (1990) Indium -bearing chalcopyrite and sphalerite from the Gåsborn area, West Bergslagen, central Sweden. Mineral Mag 54(374):109–112

Lenharo SLR, Moura MA, Botelho NF (2002) Petrogenetic and mineralization processes in Paleo- to Mesoproterozoic rapakivi granites: examples from Pitinga and Goias, Brazil. Precambrian Res 119(1–4):277–299

Lerouge C, Deschamps Y, Piantone P, Gilles Ch, Breton J (2007) Metal-carrier accessory minerals associated with W±Sn mineralization, La Chataigneraie tungsten ore district, Massif Central, France. Can Mineral 45(4):875–889

López RG (2006) Estudio Geológico-Metalogenético del área oriental al curso medio del Río Pinturas, sector noroeste del Macizo del Deseado, provincia de Santa Cruz, Argentina. Ph.D. thesis, University of La Plata. p. 206

Moreira P (2005) Geología y Metalogénesis del Distrito La Josefina, Macizo del Deseado, Santa Cruz. Ph.D. thesis, University of La Plata. p. 366

O'Leary B, Sims J (2009) Martha Mine technical report (Santa Cruz, Argentina). Coeur d'Alene Mines Corporation internal report. p. 107. Available at: www.sedar.com.

Ohmoto H, Goldhaber MB (1997) Sulfur and carbon isotopes. In: Barnes HL (ed) Geochemistry of hydrothermal ore deposits, 3rd edn. Wiley, New York, pp 517–611

Ohmoto H, Rye RO (1979) Isotopes of sulfur and carbon. In: Barnes HL (ed) Geochemistry of hydrothermal ore deposits, 2nd edn. Wiley, New York, pp 509–567

Ohta E (1995) Common features and Genesis of Tin-polymetallic veins. Resour Geol Spec Iss 18:187–195

Páez GN, Ruiz R, Guido DM, Jovic SM, Schalamuk IB (2010) The effects of K-metasomatism in the Bahía Laura Volcanic Complex, Deseado Massif, Argentina: metallogenic and petrologic consequences. Chem Geol 273:300–313

Palero-Fernández FJ, Martín-Izard A (2005) Trace element contents in galena and sphalerite from ore deposits of the Alcudia Valley mineral field (Eastern Sierra Morena, Spain). J Geochem Explor 86(1):1–25

Pankhurst R, Leat P, Sruoga P, Rapela C, Marquez M, Storey B, Riley T (1998) The Chon Aike province of Patagonia and related rocks in West Antartica: a silicic large igneous province. J Volcanol Geotherm Res 81:113–136

Pankhurst R, Riley T, Fanning C, Kelley S (2000) Episodic Silicic Volcanism in Patagonia and the Antarctic Peninsula: chronology of magmatism associated with the Break-up of Gondwana. J Petrol 41:605–625

Panza JL (1995). Hoja geológica 4969—II Tres Cerros escala 1: 250.000, Provincia de Santa Cruz. Dirección Nacional del Servicio Geológico Boletín, vol. 213. pp. 1–103

Panza JL, Haller MJ (2002). El volcanismo jurásico. In: Haller, M.J. (ed.), Geología y recursos Naturales de Santa Cruz. Relatorio del XV Congreso Geológico Argentino. pp. 89–102

Peñalva GA, Jovic SM, Chernicoff CJ, Guido DM, Schalamuk IB (2008) Cuerpos intrusivos asociados a las mineralizaciones polimetálicas del depósito Cerro León, área del anticlinal El Tranquilo, Santa Cruz: Evidencias Geofísicas. Rev Asoc Geol Argent 63(1):14–23

Plimer IR, Lu J, Kleeman JD (1991) Trace and rare earth elements in cassiterite. Sources of components for the tin deposits of the Mole Granite, Australia. Miner Deposita 26(4):267–274

Qian Z, Zhan X, Pan J, Shao S (1998) Geochemical enrichment and mineralization of indium. Chin J Geochem 17(3):221–225

Rapella CW, Pankhurst RJ (1996) Monzonite suites: the inner most Cordilleran plutonism of Patagonia. Trans R Soc Edinb Earth Sci 87:193–203

Recio C (2000) Isótopos estables en depósitos minerales. Apuntes del curso de postgrado, La Plata. p. 131

Ríos J, Alves J, Perez C, Costa E, Rosiere C, Fuzikawa K, Correia Neves J, Chaves A, Prates S, de Barrio R (2006) Combined investigations of fluid inclusions in opaque ore minerals by NIR/SWIR microscopy and microthermometry and synchrotron radiation X-ray fluorescence. Appl Geochem 21:813–819

Robinson BW, Kusakabe M (1975) Quantitative preparation of sulfur dioxide for $^{34}S/^{32}S$ analyses from sulfides by combustion with cuprous oxide. Anal Chem 47(7):1179–1181

Ruiz R, Guido DM (2006) Metal geochemistry from epithermal deposits of the Deseado Massif, Patagonia, Argentina. First International SEG Student Chapter Conference—SEG 2006, Biennial Conference "Wealth Creation in the Minerals Industry", Colorado, USA. pp. 354–355

Ruiz R, Paez GN, Guido DM, Schalamuk IB (2008) Ambiente volcánico y mineralizaciones del Área Cerro 1ro de Abril, Sector Sudoccidental del Macizo del Deseado, Santa Cruz, Argentina. XVII Congreso Geológico Argentino. Actas (2). pp. 897–898

Schalamuk IB, Zubia M, Genini A, Fernández R (1997) Jurassic epithermal Au-Ag deposits of Patagonia, Argentina. Ore Geol Rev 12(3):173–186

Schalamuk IB, de Barrio R, Zubia M, Genini A, Echeveste H (1999) Provincia Auroargentífera del Deseado, Santa Cruz. Recursos Minerales de la República Argentina In: Zappettini E (ed) Instituto de Geología y Recursos Minerales SEGEMAR, Anales, vol. 35. pp. 1177–1188

Schalamuk IB, Ríos FJ, de Barrio RE, Moreira P, Fuzikawa K, Echeveste H, Cunningham C, Vieira Alves J (2005) Mineralized fluids related to Au–Ag ores in selected districts of epithermal province Macizo del Deseado, Southern Patagonia, Argentina. XVI Congreso Geológico Argentino. Actas (2). pp. 355–360

Schwarz-Schampera U, Herzig PM (1997) Geochemistry of indium in VMS deposits. Implications from active hydrothermal vents in the southern Lau Basin (SW-Pacific). In: Papunen H (ed) Mineral deposits: research and exploration, where do they meet? Balkema, Rotterdam, pp 379–382

Schwarz-Schampera U, Herzig PM (2002) Indium. Geology, mineralogy, and economics. Springer, Berlin, p 257

Seifert T (1999) Relationship between the Late Variscan lamprophyres and hydrothermal vein mineralization in the Erzgebirge. In: Stanley CJ (ed) Mineral deposits: processes to processing, vol 1. Balkema, Rotterdam, pp 429–432

Seifert T, Sandmann D (2006) Mineralogy and geochemistry of Indium-bearing polymetallic vein-type deposits: implications for host minerals from the Freiberg district, Eastern Erzgebirge, Germany. Ore Geol Rev 28:1–31

Serranti S, Ferrini V, Masi U, Cabri LJ (2002) Trace-element distribution in cassiterite and sulfides from rubané and massive ores of the Corvo deposit, Portugal. Can Mineral 40(3):815–835

Sharpe R, Riveros C, Scavuzzo V (2002) Stratigraphy of the Chon Aike Formation ignimbrite sequence in the Cerro Vanguardia Au–Ag epithermal vein district: Actas del XV Congreso Geológico Argentino

Simmons SF, White NC, John DA (2005) Geological characteristics of epithermal precious and base metal deposits. Econ Geol 100th Anniversary Volume. pp. 485–522

Sruoga P, Busteros A, Giacosa R, Martínez H, Kleiman L, Japas S, Maloberti A, Gayone MR (2008) Análisis litofacial y estructural del Complejo Volcánico Bahía Laura en el área el Dorado-Monserrat, pcia. de Santa Cruz, Argentina. Rev Asoc Geol Argent 63(4):653–664

Tsushima N, Matsueda H, Ishihara S (1999) Polymetallic mineralization at the Nakakoshi copper deposits, central Hokkaido, Japan. Resour Geol 49(2):89–97

Wallier S (2009) The geology and evolution of the Manantial Espejo epithermal silver(–gold) deposit, Deseado Massif, Argentina. Ph. D. thesis, University British Columbia. p. 383

Zartman R, Doe B (1981) Plumbotectonics—the model. Tectonophysics 75:135–162

Zhang Q, Zhu X, He Y, Jiang J, Wang D (2006) Indium enrichment in the Meng'entaolegai Ag–Pb–Zn deposit, Inner Mongolia, China. Resour Geol 56(3):337–346

Zhang Q, Zhu X, He Y, Zhu Z (2007) In, Sn, Pb and Zn contents and their relationships in ore-forming fluids from some In-rich and In-poor deposits in China. Acta Geol Sin 81(3):450–462